Diffusion in hypo-stoichiometric uranium mononitride

Jade J. Li[a,b], Samuel T. Murphy[a,b,*]

[a]*Engineering Department, Lancaster University, Bailrigg, Lancaster, LA1 4YW, UK*
[b]*Materials Science Institute, Lancaster University, Bailrigg, Lancaster, LA1 4YW, UK*

Abstract

Uranium nitride is a nuclear fuel of interest as it offers enhanced accident tolerance, owing to its intrinsic properties. Before UN can be deployed commercially it is essential to understand its properties and how they evolve during operation. Therefore, molecular dynamics has been employed to study the study the thermal expansion and diffusivity of UN and how this changes with stoichiometry. Changes in stoichiometry are predicted to have minimal impact on the thermal expansion, however, the introduction of nitrogen vacancies does lead to a significant increase in nitrogen diffusivity.

Keywords: Diffusion, Molecular dynamics, Uranium mononitride

1. Introduction

For decades, the most widely deployed nuclear fuel in fission reactors has been uranium dioxide (UO_2), chosen for its radiation tolerance, chemical stability, compatibility with common cladding materials [1], and a high melting point of (3078 ± 15) K [2]. Due to its low thermal conductivity, uranium dioxide is vulnerable to a rapid increase in centre-line temperature and possible melting during a loss of coolant accident (LOCA), such as the 2011 incident at Fukushima Daiichi. This incident highlighted the need to improve the accident tolerance of fuels. In response, development began on, so-called, Accident Tolerant Fuels (ATFs) that are being developed as alternatives to oxide fuels, with higher thermal conductivities and specific heat capacities to extend the narrow timeframe available for operators to bring a reactor back under control. Ideally, ATFs would operate in current light-water reactors and maintain economic feasibility with improved performance relative to UO_2, such as achieving higher burn-ups [3].

One of the leading ATF candidate materials is uranium mononitride (UN), which crystallises in the $Fm\bar{3}m$ space group (No. 225), as shown in Fig. 1. This rocksalt structure consists of two interconnecting uranium and nitrogen face-centred cubic sublattices. UN exhibits a high melting point of (3120 ± 30) K and a thermal conductivity of 21 $Wm^{-1}K^{-1}$ at 2000 K [4, 5], compared to a value of 2 $Wm^{-1}K^{-1}$ for the oxide at the same temperature [6]. This significantly greater thermal conductivity reduces the rate of temperature increase in the fuel as well as ensuring lower temperature gradients and reduced thermal stresses. Furthermore, the higher uranium density of the nitride offers an economic advantage through minimising the need for enrichment with ^{235}U. However, a complicated fabrication process, requiring enrichment of ^{15}N, coupled with unfavourable reactions with hot coolant water have seen limited application compared to more conventional oxides [7].

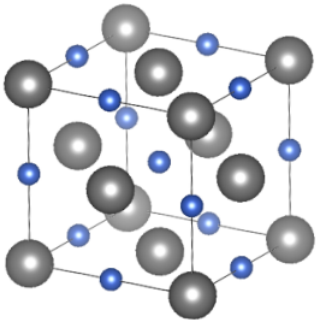

Figure 1: The structure of a UN unit cell; the larger grey and smaller blue atoms represent uranium and nitrogen, respectively. (Online version in colour.)

*Corresponding author. Department of Engineering, , Lancaster University, Lancaster, LA1 4YW, UK

Email address: samuel.murphy@lancaster.ac.uk (Samuel T. Murphy)

In current reactor designs, fuel pellets are stacked inside a cladding tube forming a fuel rod. These rods are then grouped together to form an assembly. Inside the fuel rod there is a gap between the pellet and the cladding, called the plenum, to allow for swelling of the fuel due to high temperatures and incorporation of fission products. This swelling can cause a mechanical interaction between the fuel and the cladding, which can cause cladding breach and contamination of the coolants [8]. As this is extremely undesirable, low thermal expansions are therefore required for ATFs.

Before UN can be widely deployed in reactors it is essential to understand its fundamental properties and to be able to predict how these are likely to evolve during operation. While there has been some effort to characterise UN, there is still significantly less available data than for UO_2. Hayes *et al*. have presented experimental values for the lattice parameter as a function of temperature and determined associated linear thermal expansion coefficients for UN [9–15]. Additionally, Hayes *et al*. have collated experimental values for the specific heat capacity and enthalpy as a function of temperature [14, 16–24].

Of particular interest is the mobility of the intrinsic uranium and nitrogen species in the crystal matrix, as this is expected to strongly influence the segregation of fission products. For example, iodine diffusion in UO_2 occurs on the oxygen sublattice [25, 26] and the nitrogen sublattice in UN may act in the same way. Holt and Almassy measured diffusion using single UN crystals in an α-particle activation study, and observed that for a temperature range 1900-2300 K, the mobility of nitrogen atoms was greater than that of uranium atoms [27].

Experimental activation energies for nitrogen diffusion in UN range between 1.25 eV and 4.20 eV [28, 29]. The lowest energy processes are thought to correspond to diffusion along the grain boundaries. Within the fuel grains, the nitrogen interstitial mechanism is thought to dominate with energies ranging from 2.44 eV and 2.726 eV [27–29]. However, the exact stoichiometry of the samples studied is uncertain. The U-N_2 phase diagram indicates that at low temperatures, UN is a line compound, however, at higher temperatures it is able to accommodate some nitrogen deficiency, becoming UN_{1-x} [30, 31]. This non-stoichiometry is thought to be accommodated by a combination of antisite defects and nitrogen vacancy defects [32].

As discussed above, fabrication of uranium nitride is a complex process requiring specialist facilities. Therefore, there is an impetus to utilise computer simulation to predict the properties of materials such as UN. In particular, atomistic simulation techniques have proven capable of accurately reproducing experimentally determined properties as well as providing an atomic level insight into processes such as diffusion [33–35]. Atomistic simulations fall into two broad categories, electronic structure approaches, such as density functional theory (DFT), and classical molecular dynamics (MD). Molecular dynamics uses Newton's laws of motion to evolve a system of atoms over time, with the interactions between atoms described using an empirical pair potential. It enables the prediction of a wide variety of properties, including thermal expansion and conductivity, specific heat, and mobility. Prior applications of molecular dynamics to study UN have examined the phase stability dependence on pressure [36], as well as the temperature dependence of the phononic contribution to the thermal conductivity [37]. Therefore, this work will employ molecular dynamics to examine how the introduction of nitrogen deficiency influences the thermal expansion of UN and diffusivity of nitrogen and uranium.

2. Methodology

Within a molecular dynamics simulation, the atoms are defined as point particles that interact via an empirically derived force field that is fitted to reproduce some experimentally observed properties of the crystal. In this work, the angular-dependent interatomic potential (ADP) developed for UN by Tseplyaev and Starikov is used. Energy minimisation of the uranium nitride unit cell results in a lattice parameter of 4.81 Å which compares well with an experimental lattice parameter of 4.89 Å at 53 K [38]. Furthermore, this potential has been shown to reproduce the phase transformation from $Fm\bar{3}m \rightarrow R\bar{3}m$ that occurs at 35 GPa [39]. This potential was based on the improved form of an embedded atom method potential constructed by Mishin, Mehl, and Papaconstantopoulos [40].

In a solid, diffusion is induced by the thermal hopping of atoms between sites resulting in bulk migration through the lattice. This diffusive process is typically driven by either a thermal or concentration gradient. In order to evaluate the mobility of U and N in the system, the mean squared displacement (MSD) is calculated.

The MSD is derived from Brownian motion, and is calculated as the average displacement of the atom from its initial position over a squared time interval. The diffusivity, D, can be related to the evolution of the atomic MSD over time according to:

$$\mathrm{MSD} = 2nDt, \tag{1}$$

where n represents the dimensionality of the system and t denotes time. As the UN matrix is three dimensional, $n = 3$ in this case. By calculating the diffusivity at a series of temperatures, T, and plotting as a function of $1/T$ to create an Arrhenius plot, it is possible to extract the activation energy, E_a, and the diffusion coefficient, D_0, from:

$$D = D_0 \exp\left(\frac{-E_a}{k_B T}\right), \tag{2}$$

where k_B is the Boltzmann constant.

Molecular dynamics simulations were performed using the Large-scale Atomic Molecular Massively Parallel Simulator (LAMMPS) package [41]. Simulation supercells were constructed from 15×15×15 repetitions of the unitcell [42]. The resulting supercell of 27,000 atoms combined with periodic boundaries enables a sufficient description of the infinite crystal [43]. As discussed in the introduction, the UN lattice is able to accommodate a deficiency of nitrogen at high temperatures. Therefore, to represent this hypostoichiomteric UN, antisites and nitrogen vacancies were randomly introduced, independently, into the simulation supercells using Atomsk [44]. From the phase diagram [30, 31], it can be seen that UN is able to accommodate a nitrogen content ranging from 48 - 50%, therefore we remove up to 2% of the nitrogen atoms.

Simulation supercells were initially equilibrated under isobaric conditions and at the temperature of interest for 50,000 time steps, where a single time step incremented by 1 fs. During this equilibration period, the Nosé-Hoover thermostat and barostat were applied with relaxation times of 0.1 ps and 1 ps, respectively. Following equilibration, the supercell transitioned into a microcanonical ensemble for calculation of the MSD. The MSD was calculated over 50,000 time steps for simulation supercells containing vacancy defects. For the perfect supercells and those containing antisite defects, the MSD was calculated over 1,000,000 time steps for improved statistics due to the lower level of diffusion expected. Simulations were repeated five times in order to investigate different arrangements of defects, and the standard deviations of the values from these repeated simulations were used for the error bars.

3. Results and discussion

3.1. Lattice parameter and thermal expansion

Simulations were performed across a wide temperature range. The lattice parameters for the stoichiometric and hypostoichiometric UN are plotted as a function of temperature for nitrogen vacancies in figure 2, and for antisite defects in figure 3. Also included in figures 2 and 3 is the experimental data of Hayes *et al.* [9]. Immediately obvious from the plots are an off-set of approximately 0.07 Å (1.4%) between the experimental and simulation data. This level of discrepancy is not unusual for simulations using empirical pair potentials. Despite this discrepancy, the trends in the simulation results demonstrate excellent agreement with the experimental data. All sets of data show that there is a roughly linear increase in the lattice parameter in the range 100 – 2000 K, and that the rate of increase is larger at higher temperatures.

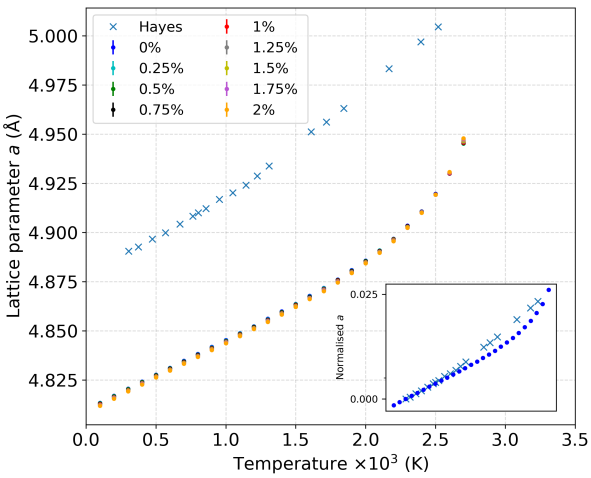

Figure 2: Lattice parameter a of UN varying with temperature at various hypo-stoichiometric values due to nitrogen vacancies. The experimental values collated in Hayes *et al.* [9] are also denoted here. The behaviour is approximately linear between 100 – 2000 K for the MD data. The inset plot demonstrates that the simulation sufficiently captures the basic material physics. The error bars are too small to see. (Online version in colour.)

The agreement between the experimental and simulation results is supported by comparing the linear thermal expansion coefficient (LTEC), α [45], which is defined

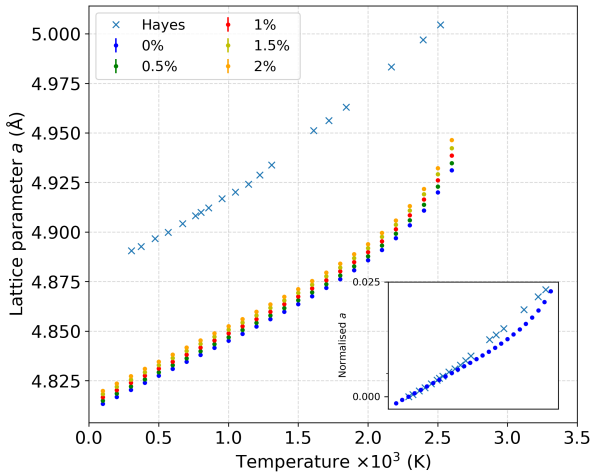

Figure 3: Lattice parameter a of UN varying with temperature at various hypo-stoichiometric values due to antisite defects. The experimental values collated in Hayes *et al.* [9] are also denoted here. The behaviour is approximately linear between 100 – 2000 K for the MD data. The inset plot demonstrates that the simulation sufficiently captures the basic material physics. The error bars are too small to see. (Online version in colour.)

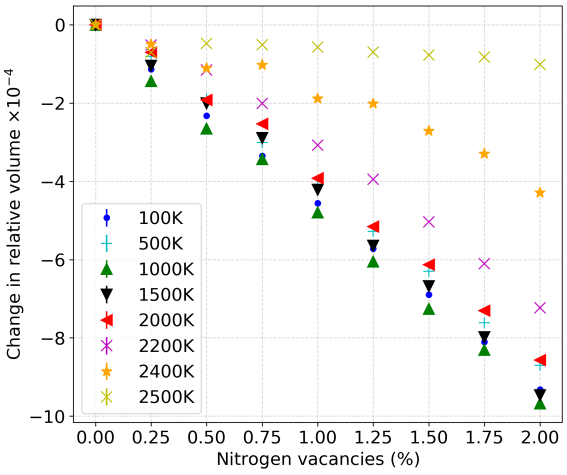

Figure 4: The change in volume relative to the volume of a perfect cell at each temperature for a supercell containing nitrogen vacancies. The error bars are too small to see. (Online version in colour.)

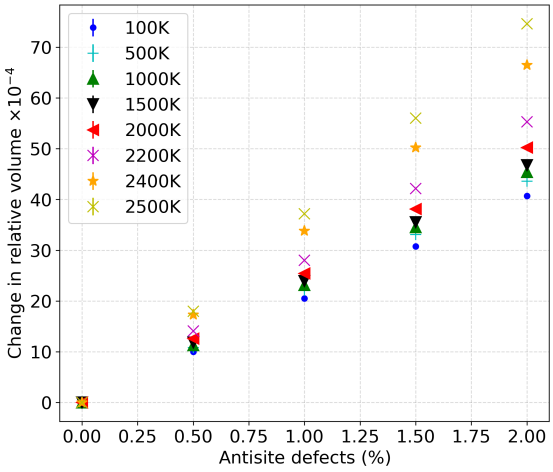

Figure 5: The change in volume relative to the volume of a perfect cell at each temperature for a supercell containing antisite defects. The error bars are too small to see. (Online version in colour.)

as the fractional change in length of an isotropic material as described by Eq. (3) [46];

$$\Delta L/L = \alpha \Delta T, \tag{3}$$

where L is the initial length of the material and ΔL is the change in length. From the simulations, a value of $(7.78 \times 10^{-6} \pm 1.91 \times 10^{-9})$ K^{-1} was determined for a defect-free supercell from the nitrogen vacancy runs, and a value of $(7.78 \times 10^{-6} \pm 5.50 \times 10^{-9})$ K^{-1} was determined for a defect-free supercell from the antisite defects runs. These values compare well with an experimental value of 7.5×10^{-6} K^{-1} across the same temperature range [9, 16, 39, 47, 48]. It is noted that these values show significant deviation (20%) from that obtained by Tseplyaev and Starikov [39]. This discrepancy may have been due to the difference in the ranges of values chosen in the calculation of the LTEC.

Also evident from figure 2 is the almost imperceptible change in the lattice parameter due to the inclusion of non-stoichiometry at all but the very highest temperatures. To examine this more closely, the relative change in volume between the non-stoichiometric and stoichiometric lattice parameters are plotted in figures 4 and 5.

Figure 4 shows that there is an almost linear decrease in the lattice parameter as the vacancy concentration increases, although the magnitude of the change decreases very slightly with temperature up until 2500 K. At this point, there is a sudden increase in the lattice parameter and there is evidence of diffusion occurring in the simulation supercell. It was also found that there is no distinctive trend between LTECs and the concentration of nitrogen vacancies, indicating that hypo-stoichiometry has a minimal effect on the expansion of UN. Figure 5 shows an almost linear increase in the lattice parameter as the amount of antisite defects increase. The data for 2500 K shows a larger increase in the lattice parameters than the lower temperatures due to the atoms possessing more energy in order to be able to diffuse through the lattice.

Prior experimental data showing the relationship between lattice parameter and the degree of non-stoichiometry is limited. Troć investigated the effect of nitrogen composition on lattice parameter and observed a decrease with an increasing amount of nitrogen interstitials at temperatures of 94 K and below [49]. In this work, lattice expansion was observed for increasing hypo-stoichiometry at temperatures above 2500 K, with lower temperatures showing lattice shrinkage for this at lower temperatures. However, Troć studied hyper-stoichiometric UN, whereas this work focuses on hypo-stoichiometric UN; these different regimes may correspond with different lattice expansion behaviours.

3.2. *Diffusion*

Intrinsic diffusion in UN was studied in the temperature range 2300–2700 K for supercells containing nitrogen vacancies and 2300-2600 K for supercells containing antisite defects only. Only the higher temperatures were considered as, due to short simulation times and small supercells, it was not possible to observe statistically significant amounts of diffusion at lower temperatures. However, as the process is Arrhenius-like, the activation energy should be similar at low temperatures, particularly when nitrogen deficiency is present. Figure 6 shows the MSD for both uranium and nitrogen as a function of time at 2500 K in a supercell containing 1.5% nitrogen vacancies. In Fig. 6, the linear increase in the MSD for nitrogen with time indicates that nitrogen is able to diffuse through the system at this temperature. By contrast, Fig. 6 shows that uranium appears to be relatively immobile even at these high temperatures.

The logarithmic diffusion as a function of inverse temperature was examined for nitrogen with different UN hypo-stoichiometry, and is shown in Fig. 7 for nitrogen vacancies, and Fig. 8 for antisite defects. As the MSD data for nitrogen atoms presented a linear trend, the method of least squares was applied to fit the nitrogen diffusion points according to Eq. (4) [50];

$$m = \frac{\sum_i (x_i - \bar{x}) y_i}{\sum_i (x_i - \bar{x})^2} = \frac{\sum_i x_i (y_i - \bar{y})}{\sum_i x_i (x_i - \bar{x})}. \qquad (4)$$

These results can be compared to diffusion plots from experiment as reported in Butt and Jaques [28] and Matzke [29]. For a perfect supercell, the diffusivity values were found to be in a similar range; a difference by an order of 10^2 can be seen between the values

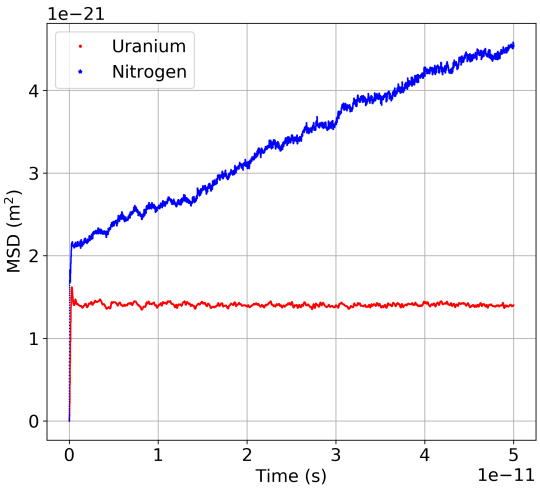

Figure 6: A plot of MSD as a function of time for a temperature of 2500 K, with 1.5% nitrogen vacancies introduced into the lattice. Error bars are present, though they are too small to be visible. (Online version in colour.)

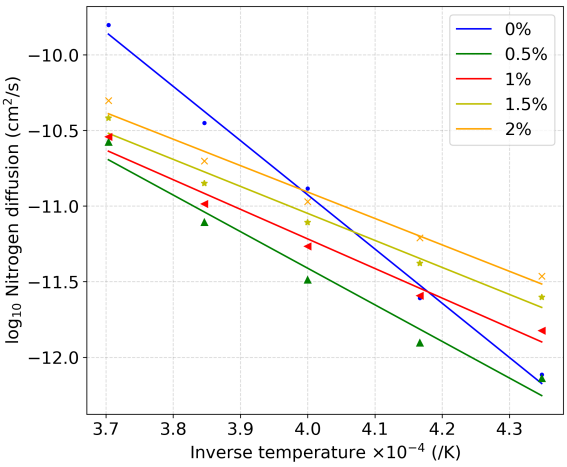

Figure 7: The logarithmic diffusion of nitrogen as a function of inverse temperature in a supercell containing nitrogen vacancies, with least squares fitting applied. The percentage of nitrogen vacancies is indicated in the legend. The error bars are too small to see. (Online version in colour.)

reported here and those reported in Matzke and Butt and Jaques. A variation of pressures may have caused this; quasi-stoichiometric UN was studied at 0.1316 atm by Matzke, however, the specify sample details were not reported, so a difference in the make up of the crystal may also have influenced this disparity.

With the gradients of the lines in Fig. 7 and Fig. 8

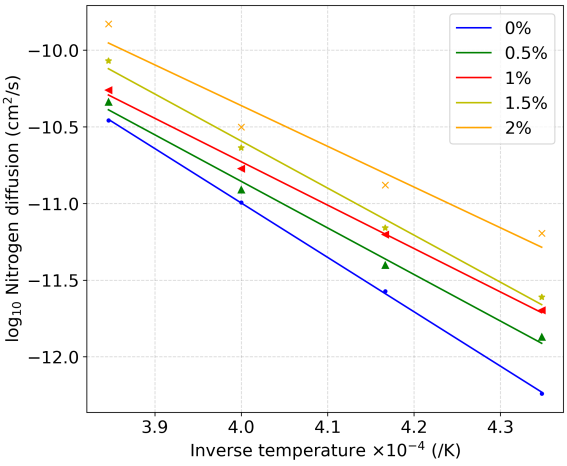

Figure 8: The logarithmic diffusion of nitrogen as a function of inverse temperature in a supercell containing antisite defects, with least squares fitting applied. The percentage of antisite defects is indicated in the legend. The error bars are too small to see. (Online version in colour.)

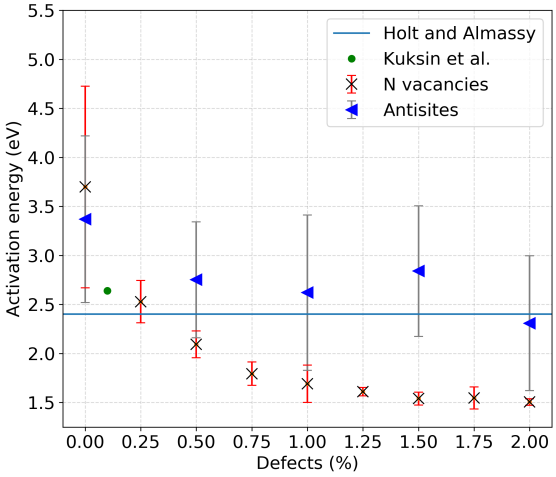

Figure 9: Nitrogen activation energies for each considered UN hypo-stoichiometry, compared to nitrogen vacancy experimental data from Holt and Almassy [27] and theoretical data from Kuksin *et al.* [51].

corresponding to the activation energies of the different systems, it is observed that most of the gradients, aside from the perfect supercell for the nitrogen vacancy case, are visibly similar, signifying similar activation energies for these systems. In Fig. 7, the gradient for the perfect supercell is steeper, which indicates a higher activation energy. This increased activation energy arises due to a lack of defects that can mediate the diffusion process in the perfect cell. The activation energies calculated using the gradients produced by the fit and Eq. (2) are displayed in Fig. 9.

Figure 9 suggests that there are multiple regimes present in the data. In stoichiometric UN, there are high corresponding nitrogen activation energies of around 3.5 eV with a relatively large error due to the relatively low levels of diffusion observed. As the concentration of defects is increased, the activation energy generally decreases, as it is easier for nitrogen diffusion to occur through defects than a defect free lattice. For higher degrees of hypo-stoichiometry, the nitrogen activation energy decreases to approximately 1.8 eV for supercells containing nitrogen vacancies, and approximately 2.6 eV for supercells containing antisite defects; this could be indicative of defect clustering, which could have an impact on the diffusivity.

An activation energy of 2.64 eV was determined for a UN sample containing 0.1% of nitrogen vacancies from previous mD simulations by Kuksin *et al.* [51], which agrees with the results presented in Fig. 9. Experimental values the activation energy for nitrogen were determined by Holt and Almassy [27]. Unfortunately, the exact level of non-stoichiometry is not reported, thereby making comparison with the simulations difficult. Figure 9 shows that both diffusion mechanisms studied exhibit similar activation energies to that of Holt and Almassy [27], but at different degrees of hypostoichiometry. At small deviations from stoichiometry (0.25%) the vacancy mechanism has an activation energy that is closer to the experiment, however, at all larger deviations the antisite results are in good agreement with experiment.

No evidence of a superionic transition (such as discontinuities in the lattice paraemters or specific heats) was observed in the simulations. Therefore, diffusion is thought to be facilitated by the thermal creation of defects in the stoichiometric and antisite containing samples and the movement of the existing defects in the vacancy containing supercells.

4. Conclusion

Thermophysical properties of hypo-stoichiometric UN have been computed using MD simulations and analysed. The lattice parameters were found to be largely unaffected by the introduction of hypostoichiometry into the lattice. The average activation energy for nitrogen in stoichiometric UN was found to be 3.54 eV, whereas for higher degrees of hypo-

stoichiometry, the activation energy decreases. If the non-stoichiometry is accommodated by vacancy defects the activation energy decreases to approximately 1.8 eV, however, accommodation by antisites results in a reduction to 2.6 eV. These values compare with an experimental value of 2.45 eV, although the exact stoichiometry of the sample is unknown. Previous work suggests that the potential predicts that the antisites are the thermodynamically most favourable process for accommodating hypostoichiometry and so are the dominant defects. The agreement between the activation energies calculated in supercells containing antisite defects and the experimental value also supports this hypothesis. This study provides a validation of material properties of UN that have been previously studied, and further material behaviours of UN can therefore be explored.

5. Acknowledgements

The authors would like to thank the High End Computing Facility at Lancaster University for the performance of simulations. This project is funded by the Leverhulme Trust [grant no. DS—2017-036] as part of the Material Social Futures programme at Lancaster University.

References

[1] M. Lyons, R. Boyle, J. Davies, V. Hazel, T. Rowland, UO_2 properties affecting performance, Journal of Nuclear Engineering and Design 21 (2) (1972) 167–199. doi:10.1016/0029-5493(72)90072-6.

[2] H. Hausner, Determination of the melting point of uranium dioxide, Journal of Nuclear Materials 15 (3) (1965) 179 – 183. doi:https://doi.org/10.1016/0022-3115(65)90178-9.
URL http://www.sciencedirect.com/science/article/pii/0022311565901789

[3] Accident Tolerant Fuel Concepts for Light Water Reactors, no. 1797 in TECDOC Series, INTERNATIONAL ATOMIC ENERGY AGENCY, Vienna, 2016.
URL https://www.iaea.org/publications/10972/accident-tolerant-fuel-concepts-for-light-water-reactors

[4] U. Carvajal Nunez, D. Prieur, R. Bohler, D. Manara, Melting point determination of uranium nitride and uranium plutonium nitride: A laser heating study, Journal of Nuclear Materials 449 (1) (2014) 1 – 8. doi:https://doi.org/10.1016/j.jnucmat.2014.02.021.
URL http://www.sciencedirect.com/science/article/pii/S002231151400083X

[5] B. Szpunar, J. A. Szpunar, Thermal Conductivity of Uranium Nitride and Carbide, International Journal of Nuclear Energy 2014 (2014) 1–7. doi:10.1155/2014/178360.

[6] Thermophysical Properties of Materials for Nuclear Engineering: A Tutorial and Collection of Data, Non-serial Publications, INTERNATIONAL ATOMIC ENERGY AGENCY, Vienna, 2009.
URL https://www.iaea.org/publications/7965/thermophysical-properties-of-materials-for-nuclear-engineering-a-tutorial-and-collection-of-data

[7] C. Ekberg, D. R. Costa, M. Hedburg, M. Jolkkonen, Nitride fuel for Gen IV nuclear power systems, Journal of Radioanalytical and Nuclear Chemistry 318 (3) (2018) 1713–1725. doi:10.1007/s10967-018-6316-0.

[8] Y. Sumi, L. Keer, S. Nemat-Nasser, Thermally induced radial cracking in fuel element pellets, Journal of Nuclear Materials 96 (1) (1981) 147 – 159. doi:https://doi.org/10.1016/0022-3115(81)90228-2.
URL http://www.sciencedirect.com/science/article/pii/0022311581902282

[9] S. L. Hayes, J. K. Thomas, K. L. Peddicord, Material property correlations for uranium mononitride: I. Physical properties, Journal of Nuclear Materials 171 (1990) 262–270. doi:10.1016/0022-3115(90)90374-V.

[10] R. Benz, G. Balog, B. H. Baca, High Temperature Science 15 (1970) 221.

[11] C. P. Kempter, R. O. Elliott, Thermal Expansion of ⟨UN⟩,⟨UO_2⟩, ⟨UO_2·ThO_2⟩, and ⟨ThO_2⟩, The Journal of Chemical Physics 30 (6) (1959) 1524–1526. arXiv:https://doi.org/10.1063/1.1730230, doi:10.1063/1.1730230.
URL https://doi.org/10.1063/1.1730230

[12] F. L. Carlsen, W. O. Harms, Thermal expansion of UN, Tech. Rep. ORNL-3670, Oak Ridge National Laboratory (1964).

[13] K. M. Taylor, C. H. McMurtry, SYNTHESIS AND FABRICATION OF REFRACTORY URANIUM COMPOUNDS. Summary Report for May 1959 through December 1960doi:10.2172/4843747.
URL https://www.osti.gov/biblio/4843747

[14] E. O. Speidel, D. L. Keller, B. M. Institute., U. A. E. Commission., Fabrication and properties of hot-pressed uranium mononitride, UC (Series). 25, Metallurgy, Ceramics and Materials, Battelle Memorial Institute ; Available from Office of Technical Services, U.S. Dept. of Commerce, Columbus, OH : Washington, D.C., 1963, 66 p.
URL //catalog.hathitrust.org/Record/100168477

[15] R. Holden, U. A. E. Commission, A. S. for Metals, Ceramic Fuel Elements, (An AEC Monograph), Gordon and Breach, 1966.

[16] S. L. Hayes, J. K. Thomas, K. L. Peddicord, Material property correlations for uranium mononitride: IV. Thermodynamic properties, Journal of Nuclear Materials 171 (2) (1990) 300–318. doi:https://doi.org/10.1016/0022-3115(90)90377-Y.
URL https://www.sciencedirect.com/science/article/pii/002231159090377Y

[17] J. F. Counsell, R. M. Dell, J. F. Martin, Thermodynamic properties of uranium compounds. Part 2.—Low-temperature heat capacity and entropy of three uranium nitrides, Trans. Faraday Soc. 62 (1966) 1736–1747. doi:10.1039/TF9666201736.
URL http://dx.doi.org/10.1039/TF9666201736

[18] E. F. Westrum Jr, C. M. Barber, Uranium mononitride: Heat capacity and thermodynamic properties from 5 to 350 K, The Journal of Chemical Physics 45 (2) (1966) 635–639.

[19] E. Cordfunke, R. Muis, The heat capacity of uranium mononitride, Journal of Nuclear Materials 42 (2) (1972) 233–234.

[20] C. Affortit, Chaleur specifique de UC et UN, Journal of Nuclear Materials 34 (1) (1970) 105–107.

[21] Y. Takahashi, M. Murabayashi, Y. Akimoto, T. Mukaibo, Uranium mononitride: heat capacity and thermal conductivity from 298 to 1000 K, Journal of Nuclear Materials 38 (3) (1971) 303–308.

[22] J. Conway, P. N. Flagella, PHYSICAL AND MECHANICAL

PROPERTIES OF REACTOR MATERIALS, 1969.

[23] W. Fulkerson, T. G. Kollie, S. C. Weaver, J. P. Moore, R. K. Williams, ELECTRICAL AND THERMAL PROPERTIES OF THE NaCl STRUCTURED METALLIC ACTINIDE COMPOUNDS, Nucl. Met., Met. Soc. AIME 17: 374-85(1970).
URL https://www.osti.gov/biblio/4080260

[24] F. L. Oetting, J. M. Leitnaker, The chemical thermodynamic properties of nuclear materials I. uranium mononitride, The Journal of Chemical Thermodynamics 4 (2) (1972) 199–211.

[25] M. W. D. Cooper, S. T. Murphy, P. C. M. Fossati, M. J. D. Rushton, R. W. Grimes, Thermophysical and anion diffusion properties of $(U_x,Th_{1-x})O_2$, Proceedings of the Royal Society A: Mathematical, Physical and Engineering Sciences 470 (2171) (2014) 20140427. doi:10.1098/rspa.2014.0427.
URL https://doi.org/10.1098/rspa.2014.0427

[26] R. W. Grimes, C. R. A. Catlow, The Stability of Fission Products in Uranium Dioxide, Philosophical Transactions: Physical Sciences and Engineering 335 (1639) (1991) 609–634.
URL http://www.jstor.org/stable/53802

[27] J. B. Holt, M. Y. Almassy, Nitrogen Diffusion in Uranium Nitride as Measured by Alpha Particle Activation of ^{15}N, Journal of the American Ceramic Society 52 (1969) 631–635. doi:10.1111/j.1151-2916.1969.tb16064.x.

[28] D. P. Butt, B. Jaques, Synthesis and Optimization of the Sintering Kinetics of Actinide Nitridesdoi:10.2172/953344.

[29] H. Matzke, Atomic mechanisms of mass transport in ceramic nuclear fuel materials, Journal of the Chemical Society, Faraday Transactions 86 (8) (1990) 1243–56. doi:10.1039/ft9908601243.

[30] L. Olivares, J. Lisboa, J. Marin, M. Barrera, A. Navarrete Villegas, Atomization of UMo Particles under Nitrogen Atmosphere, World Journal of Nuclear Science and Technology 06 (2016) 43–52. doi:10.4236/wjnst.2016.61004.

[31] H. Okamoto, N-U (Nitrogen-Uranium), Journal of Phase Equilibria 18 (1) (1997) 107. doi:10.1007/BF02646768.
URL https://doi.org/10.1007/BF02646768

[32] S. Starikov, M. Korneva, Description of phase transitions through accumulation of point defects: UN, UO_2 and UC, Journal of Nuclear Materials 510 (2018) 373 – 381. doi:https://doi.org/10.1016/j.jnucmat.2018.08.025.
URL http://www.sciencedirect.com/science/article/pii/S0022311518300709

[33] J. E. Garcés, G. Bozzolo, Atomistic Simulation of High-Density Uranium Fuels, Science and Technology of Nuclear Installations 2011 (2011) 531970. doi:10.1155/2011/531970.
URL https://doi.org/10.1155/2011/531970

[34] Y. Mishin, An Atomistic View of Grain Boundary Diffusion, Defect and Diffusion Forum 363 (2015) 1–11. doi:10.4028/www.scientific.net/ddf.363.1.
URL http://dx.doi.org/10.4028/www.scientific.net/DDF.363.1

[35] R. Mohammadzadeh, M. Mohammadzadeh, Grain boundary and lattice diffusion in nanocrystal α-iron: An atomistic simulation study, Physica A: Statistical Mechanics and its Applications 482 (2017) 56–64. doi:https://doi.org/10.1016/j.physa.2017.04.070.
URL https://www.sciencedirect.com/science/article/pii/S0378437117303801

[36] Y. Li, J. Cai, D. Mo, Molecular dynamics simulations on the effect of nanovoid on shock-induced phase transition in uranium nitride, Physics Letters A 383 (5) (2019) 458 – 463. doi:https://doi.org/10.1016/j.physleta.2018.11.017.
URL http://www.sciencedirect.com/science/article/pii/S0375960118311629

[37] K. Kurosaki, K. Yano, K. Yamada, M. Uno, S. Yamanaka, A molecular dynamics study of the thermal conductivity of uranium mononitride, Journal of Alloys and Compounds 311 (2) (2000) 305 – 310. doi:https://doi.org/10.1016/S0925-8388(00)01127-0.
URL http://www.sciencedirect.com/science/article/pii/S0925838800011270

[38] H. W. Knott, G. H. Lander, M. H. Mueller, O. Vogt, Search for lattice distortions in UN, UAs, and USb at low temperatures, Phys. Rev. B 21 (1980) 4159–4165. doi:10.1103/PhysRevB.21.4159.
URL https://link.aps.org/doi/10.1103/PhysRevB.21.4159

[39] V. Tseplyaev, S. Starikov, The atomistic simulation of pressure-induced phase transition in uranium mononitride, Journal of Nuclear Materials 480 (2016) 7 – 14. doi:https://doi.org/10.1016/j.jnucmat.2016.07.048.
URL http://www.sciencedirect.com/science/article/pii/S002231151630469X

[40] Y. Mishin, Interatomic Potentials for Metals, Springer Netherlands, Dordrecht, 2005, pp. 459–478. doi:10.1007/978-1-4020-3286-8_23.
URL https://doi.org/10.1007/978-1-4020-3286-8_23

[41] S. Plimpton, Fast Parallel Algorithms for Short-Range Molecular Dynamics, Journal of Computational Physics 117 (1995) 1–19. doi:10.1006/jcph.1995.1039.

[42] S. Gražulis, A. Daškevič, A. Merkys, D. Chateigner, L. Lutterotti, M. Quirós, N. R. Serebryanaya, P. Moeck, R. T. Downs, A. Le Bail, Crystallography Open Database (COD): an open-access collection of crystal structures and platform for world-wide collaboration, Nucleic Acids Research 40 (D1) (2012) D420–D427. arXiv:http://nar.oxfordjournals.org/content/40/D1/D420.full.pdf+html, doi:10.1093/nar/gkr900.
URL http://nar.oxfordjournals.org/content/40/D1/D420.abstract

[43] R. E. Rundle, N. C. Baenziger, A. S. Wilson, R. A. McDonald, The Structures of the Carbides, Nitrides and Oxides of Uranium, Journal of the American Chemical Society 70 (1948) 99–105. doi:10.1021/ja01181a029.

[44] P. Hirel, Atomsk: A tool for manipulating and converting atomic data files, Computer Physics Communications 197 (2015) 212 – 219. doi:https://doi.org/10.1016/j.cpc.2015.07.012.
URL http://www.sciencedirect.com/science/article/pii/S0010465515002817

[45] W. Callister, D. Rethwisch, Materials Science and Engineering: An Introduction, 8th Edition, Wiley, 2009.

[46] W. F. Hosford, Mechanical Behavior of Materials, 2nd Edition, Cambridge University Press, 2009. doi:10.1017/CBO9780511810923.

[47] H. Matzke, Science of advanced LMFBR fuels, North-Holland, Netherlands, 1986.
URL http://inis.iaea.org/search/search.aspx?orig_q=RN:18075875

[48] M. Salleh, J. E. MacDonald, G. Saunders, P. d. V. Du Plessis, Hydrostatic pressure dependences of elastic constants and vibrational anharmonicity of uranium nitride, Journal of Materials Science 21 (7) (1986) 2577–2580.

[49] R. Troć, Magnetic susceptibility of the uranium nitrides, Journal of Solid State Chemistry 13 (1) (1975) 14 – 23. doi:https://doi.org/10.1016/0022-4596(75)90076-6.
URL http://www.sciencedirect.com/science/article/pii/0022459675900766

[50] I. Hughes, T. P. A. Hase, Measurements and their uncertainties: a practical guide to modern error analysis, Oxford Oxford University Press, 2011.

[51] A. Y. Kuksin, S. V. Starikov, D. E. Smirnova, V. I. Tseplyaev, The diffusion of point defects in uranium mononitride: Combination of DFT and atomistic simulation with novel potential, Journal of Alloys and Compounds 658 (2016) 385 – 394. doi:https://doi.org/10.1016/j.jallcom.2015.10.223. URL http://www.sciencedirect.com/science/article/pii/S0925838815314791